Li *et al. Cancer Cell International* (2026) 26:152
https://doi.org/10.1186/s12935-026-04244-z

Cancer Cell International

RESEARCH Open Access

# PIEZO1 enhances pancreatic cancer neurotropism

Jinhong Li[1,2], Qicai Liu[1,3], Renfeng Xu[1], Juan Tang[4], Ling Wang[4], Yuqing Zheng[4], Shangeng Weng[5] and Feng Gao[4,6*]

**Abstract**

Perineural invasion (PNI), as a prominent feature of pancreatic ductal adenocarcinoma, is closely related to poor prognosis and urgently needs to be investigated mechanisms to find effective intervention measures. PIEZO1, a mechanically activated cation channel, has emerged as a protein of interest in cancer research. This study aimed to elucidate the role of PIEZO1 in pancreatic cancer, with a particular focus on its association with neural invasion. Spatial transcriptome analysis of pancreatic cancer tissue samples revealed that PIEZO1 expression was significantly elevated in perineural invasion areas compared to non-perineural regions. Furthermore, PIEZO1 expression exhibited a gradient decrease from the vicinity of perineural invasion sites to more distant areas. Functional analyses and co-culture assays revealed that PIEZO1 activation consolidates a neurotrophic, neuroinvasive phenotype in pancreatic cancer cells. Transcriptomic analysis linked PIEZO1 to the Hippo signaling pathway, identifying YAP1 as a potential transcriptional target. In vivo studies showed that PIEZO1 inhibition reduced PNI and liver metastasis in mice. Collectively, these results identify PIEZO1 as a key contributor to PNI in pancreatic cancer and suggest that the PIEZO1-YAP1 axis warrants further exploration as a candidate signaling module for future therapeutic strategies.

**Keywords** Pancreatic cancer, Perineural invasion, PIEZO1, YAP1, Transcriptomic analysis

## Introduction

Pancreatic cancer (PC) is a devastating disease with a notoriously poor prognosis [1]. The five-year survival rate for pancreatic cancer is less than 10%, and most patients experience severe abdominal pain in the advanced stages of the disease [2]. This pain has been shown to have a significant impact on the quality of life of patients, and there is even evidence to suggest that it can lead to an increased risk of substance abuse [3]. Perineural invasion (PNI) is now recognized as the principal driver of neuroinflammation and neuropathic pain in PDAC [4]. In Pancreatic Ductal Adenocarcinoma (PDAC), perineural infiltration is present in up to 100% of cases [5, 6]. PNI is one of the significant causes of recurrence and metastasis after pancreatic cancer resection and an independent prognostic indicator [7], but its specific mechanism in PDAC is unknown. Consequently, further elucidation

†Li Jinhong and Liu Qicai are co-first authors.

*Correspondence:
Feng Gao
fengfang77777@163.com
[1]Department of Reproductive Medicine Center, The First Affiliated Hospital, Fujian Medical University, Fuzhou, P. R. China
[2]Department of Clinical Laboratory, Fujian Medical University Union Hospital, Fuzhou, P. R. China
[3]Hepatopancreatobiliary Center, Beijing Tsinghua Changgung Hospital, Institute for Precision Medicine, Key Laboratory of Digital Intelligence Hepatology (Ministry of Education), Tsinghua University, Beijing, P. R. China
[4]Department of Pathology, The First Affiliated Hospital, Fujian Medical University, Fuzhou, P. R. China
[5]Department of Hepatopancreatobiliary Surgery, The First Affiliated Hospital, Fujian Medical University, Fuzhou, P. R. China
[6]Department of Pathology, Binhai Campus of the First Affiliated Hospital, National Regional Medical Center, Fujian Medical University, Fuzhou, P. R. China

© The Author(s) 2026. **Open Access** This article is licensed under a Creative Commons Attribution-NonCommercial-NoDerivatives 4.0 International License, which permits any non-commercial use, sharing, distribution and reproduction in any medium or format, as long as you give appropriate credit to the original author(s) and the source, provide a link to the Creative Commons licence, and indicate if you modified the licensed material. You do not have permission under this licence to share adapted material derived from this article or parts of it. The images or other third party material in this article are included in the article's Creative Commons licence, unless indicated otherwise in a credit line to the material. If material is not included in the article's Creative Commons licence and your intended use is not permitted by statutory regulation or exceeds the permitted use, you will need to obtain permission directly from the copyright holder. To view a copy of this licence, visit http://creativecommons.org/licenses/by-nc-nd/4.0/.

of tumor-nerve interactions and targeted studies of PNI may yield novel therapeutic strategies to enhance the prognosis of PDAC patients.

The tumor microenvironment has been demonstrated to play a pivotal role in PNI. The TME in PDAC is characterized by a dense desmoplastic stroma and significant immune cell infiltration, creating a complex ecosystem that influences tumor progression and therapeutic response [8, 9]. Atomic force microscopy analysis has shown that the stiffness of pancreatic cancer tissue (6 kPa) significantly exceeds that of normal pancreatic tissue (1–3 kPa) [10]. Increased tumor stromal stiffness has been demonstrated to correlate with disease progression and aggressiveness and is associated with an unfavorable prognosis for patients [11, 12]. Increased tumor stromal stiffness can promote PNI by inducing cancer cells to express pro-metastatic and neurotrophic factors [13]. Furthermore, the over-expression of Yes-associated protein 1 (YAP1) has been observed to promote PNI in prostate cancer [14]. YAP1, a critical transcription factor in the intracellular mechanosensing apparatus, suggests that increased stromal stiffness may be a significant risk factor for cancer microinvasion [15]. Critically, the transduction of extracellular mechanical cues (such as matrix stiffness) into intracellular biochemical signals is often initiated by mechanosensitive ion channels at the cell membrane. Among these, the Piezo-type mechanosensitive ion channel component 1 (PIEZO1) has emerged as a key molecular sensor that is directly activated by elevated matrix stiffness [16, 17].

PIEZO1 is a multichannel transmembrane protein with significant conservation across vertebrates [18]. PIEZO1 possesses distinct ion channel characteristics responsive to mechanical stimuli, such as membrane stretch, shear flow, matrix stiffness, and tissue compression. This stimulation leads to non-selective cation permeabilization, with calcium ($Ca^{2+}$) being the predominant ion affected [19]. $Ca^{2+}$ is a second messenger that regulates various cellular functions, including metabolism, proliferation, migration, angiogenesis, and cytoskeletal remodeling [20]. Consequently, PIEZO1 has been identified as a critical mediator that connects mechanical forces to biological signals. While research has revealed that PIEZO1 expression is notably elevated in pancreatic cancer and is associated with an adverse patient prognosis, and may even act as a potential oncogene in disease progression [21], its specific role in the critical process of PNI has not been determined. In addition, the importance of PIEZO1 in Schwann cell-mediated axon repair and regeneration has been investigated [22], suggesting a plausible link to nerve-related pathology. The effect of PIEZO1 on PNI in PC and its underlying mechanisms are unknown and thus constitute the focus of the present study.

Based on the established link between matrix stiffness and PNI, and the role of PIEZO1 as a key mechanosensor, we hypothesized that the mechanically activated ion channel PIEZO1 drives perineural invasion in pancreatic cancer by activating the YAP1 signaling pathway, thereby promoting a neurotrophic and invasive phenotype in cancer cells.While PIEZO1 has been implicated in pancreatic cancer progression and YAP1 activation in other tumor contexts, its specific involvement in PNI—a key mechanism of metastasis and pain in PDAC—remains poorly understood. Prior studies have not spatially or functionally characterized PIEZO1 within the perineural niche, nor have they elucidated the mechanistic basis by which PIEZO1-mediated mechanotransduction facilitates neuroinvasion. This study aims to address this knowledge gap by investigating whether PIEZO1, through YAP1 signaling, regulates the neurotropic behavior of pancreatic cancer cells—a question with direct relevance to PDAC-associated pain and recurrence. The present study set out to systematically elucidate the molecular mechanism of PIEZO1 in pancreatic cancer neuroinvasion and its clinical significance. Utilizing a multifaceted approach encompassing bioinformatics analysis, spatial transcriptomics, in vitro functional experiments, and in vivo xenograft models, we ascertained that PIEZO1 demonstrated heightened expression in pancreatic cancer tissues, particularly near tumor-infiltrating nerves. Further mechanistic studies revealed that PIEZO1 may induce epithelial-mesenchymal transition (EMT) by activating the Hippo/YAP1 signaling pathway, thereby driving active invasion of nerves by cancer cells. These findings support the hypothesis that the PIEZO1-Hippo/YAP1 axis may contribute to pancreatic cancer neuroinvasion and warrant further exploration as a candidate signaling module in future mechanistic and therapeutic studies.

## Materials and methods

### Clinical specimens and cell culture

The human pancreatic cancer cell lines Panc-1 and Bxpc-3, as well as rat adrenal pheochromocytoma cells (PC12), were purchased from Wuhan Puno Saibu Science and Technology Co. BxPc-3 and PC12 cells were cultivated in RPMI-1640. In contrast, PANC-1 cells were grown in DMEM. The culture medium contained 10% fetal bovine serum (FBS, Invitrogen), 100 U/ml penicillin, and 100ug/ml streptomycin (Invitrogen). The culture conditions were 5% $CO_2$ and 37 °C cell culture incubator. Yoda1 (HY-18723, MedChemExpress, USA) and GsMTx4 (HY-P1410, MedChemExpress, USA) were purchased from MedChemExpress. For PIEZO1 activation, Yoda1 was used at 10 μM based on dose-response experiments (Fig. S1). For inhibition, GsMTx4 was applied at 2.5 μM. Both compounds were dissolved in DMSO and treatments lasted 24 h unless specified otherwise. A total of

20 pancreatic cancer tissues and 20 matched paracarcinoma sections were obtained from the Department of Pathology of the First Hospital of Fujian Medical University. The study was conducted following the Declaration of Helsinki and all protocols were approved by the Ethics Committee of The First Hospital of Fujian Medical University under the ethical approval numbers 2018 [053] and 2024 [714].

#### Histopathological analysis

Immunohistochemical staining of paraffin sections was performed using the affinity-biotin-dab complex method. Briefly, immunohistochemical staining of paraffin sections was performed with PIEZO1 (15939-1, Proteintech, China), YAP1 (A19134, ABclonal, China), NGF (ET1606-29, HUABIO, China), BDNF (CY5577, Abways, China), GDNF (CY6856, Abways, China), E-Cadherin (20874-1-AP, Proteintech, China), N-Cadherin (22018-1-AP, Proteintech, China) specific primary antibodies was incubated overnight at 4 °C and then incubated with biotin-coupled goat anti-rabbit secondary antibody (SA00004-2, CA, Proteintech, China) followed by streptavidin-coupled horseradish peroxidase (PR30015, Proteintech, China), DAB peroxidase substrate (PR30010, Proteintech, China) for visualisation. And the specimens were counterstained with hematoxylin (H9627, Sigma Chemical). A total of 20 pancreatic cancer tissue samples and 20 paracarcinoma sections were used for immunohistochemical analysis, with each experiment repeated three times to ensure reproducibility.

#### Immunofluorescence staining

Tissue samples from cases of pancreatic cancer were subjected to a series of processing steps, including dewaxing, rehydration, and antigen repair. Following this, the samples were incubated with primary antibodies specific to PIEZO1 (15939-1, Proteintech, China), S100β (ET1610-3, HUABIO, China), and MUC1 (GB14077-50, Servicebio, China). These incubations were conducted at 4 °C for 16 h. The cells were transferred to a new solution and incubated overnight at 4 °C. The secondary antibody was diluted 200-fold in a wet box at room temperature and protected from light for one hour. Subsequently, the nuclei of the cells were re-stained with 4',6-diamidino-2-phenylindole (DAPI), and the expression of fluorescent markers was observed utilising an orthogonal fluorescence microscope. The resulting images were captured. For tissue immunofluorescence, 20 pancreatic cancer samples were used, with each sample analyzed in triplicate.

The inoculation of pancreatic cancer cells was conducted on cell crawls at 2–4 × 104 cells/ml density. Upon completion of the intervention culture, the medium was removed, and the cells were fixed with 4% paraformaldehyde. Subsequently, the cells were treated with 0. The cells were then subjected to a 2% TritonX-100 membrane-breaking treatment, followed by an overnight incubation at 4 °C with an anti-YAP-1 monoclonal antibody. The cells were incubated with a CY3-coupled goat-anti-rabbit IgG fluorescent secondary antibody (BA1032, Boster, China) at room temperature and protected from light for one hour. To observe the nuclear translocation of Yap-1, the cell nuclei were stained with DAPI, and the samples were examined using a fluorescence microscope (OLYMPUS BX53, Japan). All cell-based immunofluorescence experiments were performed with $n = 3$ independent replicates.

#### Spatial transcriptome analysis

Spatial transcriptomics analysis of human pancreatic cancer tissue specimens was performed using the 10x Genomics Visium platform. A total of 3 pancreatic cancer tissue samples were used for spatial transcriptomics analysis. The spatial resolution was 55 μm, capturing transcriptome-wide data from defined tissue regions. The tissue sections were hybridised to spatial barcode probes, after which total RNA was extracted for library preparation. After this, sequencing was performed on the NovaSeq 6000 platform. Normalisation, feature detection, and spatial cell type annotation were then carried out using Cell Ranger and Seurat. Regions of interest were defined based on H&E staining: PNI regions (tumor cells directly adjacent to nerves), peri-PNI regions (within 200 μm of nerves), and non-PNI regions (distant from nerves). Batch effects were corrected using Seurat's integration workflow. Differential expression analysis used a threshold of FDR < 0.05 and |log2FoldChange| > 1.

#### Wound-healing assay

The logarithmic growth of Panc1 and Bxpc3 cells was initiated by inoculation in 12-well plates. Following full growth, the cells were subjected to a 12-hour starvation period in a serum-containing 1% FBS basal medium. A lance tip was used at an angle of 30° to create a scratch wound, and the wounds were observed under a microscope to ascertain their homogeneity. The de-walled cells were then washed off using PBS. Thereafter, 2 ml of complete medium containing the agonist or inhibitor was added, and the samples were incubated in a 37℃, 5% $CO_2$ incubator for 18–24 h. An inverted phase contrast microscope was utilised for observation and image capture, and ImageJ software was employed to analyse the area of scratches.

#### Transwell assay

The invasive capability of pancreatic cancer cells was assessed using the Transwell assay, wherein the upper chamber was pre-coated with matrix gel (0827065,

ABW). Cancer cells were inoculated in a serum-free medium within the upper chamber, while the lower chamber was filled with 10% FBS medium. Following a 24-hour incubation at 37℃, the migrated cells were subjected to fixation with 4% paraformaldehyde and staining with 0.1% crystal violet. Photographs were then taken through a microscope with a magnification of 100×.

When the neuromigration ability of pancreatic cancer cells was assessed using the Transwell assay, the lower chamber was pre-inoculated with PC12 cells. The cancer cells were inoculated in a serum-free medium in the upper chamber, and a serum-free medium was added to the lower chamber. Following incubation at 37℃ for 24 h, the migrated cells were fixed with 4% paraformaldehyde and stained with 0.1% crystal violet. Photographs were then taken through a microscope with a magnification of 100×.

#### RT-qPCR

Total RNA was extracted from cells using an RNA extraction kit (R711-01, Vazyme, China). First-strand cDNA was synthesised using a FastKing RT Kit (with gDNase) Reverse Transcription Kit (KR123, TIANGEN, China). mRNA relative expression was detected on a 7500 real-time fluorescent quantitative PCR instrument using a RealUniversal colour fluorescent quantitative Pre-mixing kit (FP201, TIANGEN, In the present study, the relative expression of mRNA was detected on a 7500 real-time fluorescence quantitative PCR instrument. The Ct value of the RT-qPCR product of the target gene amplified in the samples was obtained from ABI7500 software for relative quantification. The results were expressed as 2-△△Ct (whereby 2-△△Ct = Ct value of the target gene - Ct value of the internal reference gene). Ct value, or ΔΔCt, is calculated as follows: (experimental group ΔCt - control group ΔCt).

#### Western blot

After collecting cells, the total protein was extracted with cell lysate (AR0102-10, Boster, China). The total protein concentration was determined using the BCA Protein Concentration Assay Kit, separated by 10% SDS-PAGE, and transferred to a PVDF membrane. The membranes were closed using 5% skimmed milk, and then the membranes were incubated with anti-E-Cadherin polyclonal antibody, N-Cadherin polyclonal antibody, NGF polyclonal antibody, BDNF polyclonal antibody, GDNF polyclonal antibody, anti-YAP-1, β-tubulin (ET1602-4, Huabio, China), GAPDH ( AF1186, Bioss, China) and Histone H3-specific primary antibody were incubated in a shaker at 4 °C overnight, washed three times with TBST, and then incubated with HRP-coupled goat anti-rabbit IgG secondary antibody (Bs-0295, Bioss, China) for one h at room temperature. Finally, the ECL chemiluminescence kit (AR1190, Boster, China) was exposed for imaging in a Bio-Rad gel imager.

#### Perineural invasion test

PC12 cells were inoculated in 2 ul growth factor-reduced matrix gel ($2 \times 10^4$ cells/drop). PC cells were labelled with 25 μM fluorescent CellTracker Green CMFDA (40721ES60, YEASEN, China) for one hour at 37 °C and then co-cultured with differentiated neurons or neuron-like cells for 4 days around the stroma at a dose of $1–2 \times 10^5$ cells/drop. Autonomous invasion of cancer cells was monitored by parallel incubation with 2ul of blank matrix gel under the same experimental conditions. After the experiment, the culture medium was removed, and the samples were washed thrice with PBS. Fluorescent images were then acquired using a fluorescence microscope. The presence of PC cells invading nerves was defined as fluorescent cancer cells associated with neural synapses embedded in stromal gel. The degree of PNI of PC cells was calculated by subtracting the fluorescence signal produced by cancer cells invading stromal gel in tumour-neuronal cell co-cultures from the fluorescence signal generated by cancer cells cultured in parallel with blank stromal gel alone by ImageJ software.

#### Nerve attachment assay

PC12 cells were inoculated at high density in 24-well plates and cultured for 3–5 days to spread over the bottom of the wells to form a uniform single-cell layer of neuronal cells. The PC cells were labelled with 25 μM fluorescent CellTracker Green CMFDA at 37 °C for one hour. Agonists or inhibitors were added to the cell suspension and then inoculated uniformly at $1 \times 10^5$/well into the wells of a 24-well plate spread with neuronal cells. The plate was then incubated in a 5% $CO_2$-saturated humidity incubator at 37 °C for 45 min. The culture medium and unadhered cells were then discarded. The serum-free DMEM culture medium was then washed gently on one occasion. Fluorescence images were then acquired using a fluorescence microscope.

#### RNA-seq

Total RNA was extracted from the cells using Trizol (15596018CN, Invitrogen) according to the instructions. RNA integrity was assessed using an Agilent 2100 Bioanalyzer (all samples had RIN > 8.0). Library preparation and sequencing were performed by Shenzhen Huada Genetics on the NovaSeq 6000 platform (Illumina) with 150 bp paired-end reads. Raw sequencing data were processed as follows: adapter sequences and low-quality reads (Phred score < 20) were trimmed using cutadapt (version 1.11). Clean reads were aligned to the human reference genome (GRCh38) using HISAT2 (version 2.1.0). Gene expression quantification was performed

using featureCounts (v1.6.0), and expression values were normalized as FPKM (Fragments Per Kilobase of transcript per Million mapped reads). To ensure robust comparisons across samples, we applied the TMM (Trimmed Mean of M-values) normalization method within the edgeR package. Potential batch effects were assessed and corrected using the removeBatchEffect function in the limma R package, which is a standard approach for ensuring data integrity in transcriptomic studies. Differential expression analysis was conducted using edgeR with a generalized linear model, applying a threshold of FDR < 0.05 and |log2FoldChange| > 1 to identify statistically significant genes. Functional enrichment analysis (GO and KEGG) was performed using ClusterProfiler with a hypergeometric test (p-value cutoff of 0.05). The resulting sequencing data have been deposited in the NCBI Sequence Read Archive (SRA) for public access and the GEO accession number for the sequencing data is PRJNA1348867.

### Mouse sciatic nerve injection

The experiment used 4–6-week-old nude mice from the Wu Animal Center, Fuzhou, China. All animal experiments in this study were approved by the Ethics Committee (Approval No. IACUCBWS24090701) and performed strictly following the Guide for the Care and Use of Laboratory Animals. Mice were randomly assigned to control and treatment groups ($n = 6$ per group) using a random number table. Investigators were blinded to group allocation during data collection and analysis. The mice were anaesthetised, and the right lower limbs of BALB/C mice were sterilised. A 3–4 mm incision was then made along the femoral stem alignment at 1–2 mm below the femoral head of the right lower limb. The muscle was peeled off along the muscle alignment, the sciatic nerve was searched for and exposed, and 1 million Bxpc3 cells (1:1 mixed stromal gel) around the sciatic nerve, respectively, and then sewed up the incision, and dynamically observed the tumorigenic situation and the time of tumorigenicity. The mice underwent pharmacological intervention once the tumours became palpable (approximately 1 week after injection). The tumours were injected in situ with 200 μM×10 μL GsMTx4 or an equivalent volume of PBS, administered every three days for three weeks. After the experiment, the mice were euthanised by cervical dislocation, and the tumours, livers, and lungs were extracted and placed in 4% paraformaldehyde for adequate fixation. The tissues were then routinely paraffin-embedded and subjected to HE staining for the presence of PNI and metastasis. The ethical approval number for this study was IACUCBWS24090701.

### Statistical analysis

Comparisons between two groups that satisfied normal distribution and variance chi-square were performed using independent samples t-test; comparisons between more than three groups were performed using analysis of variance (ANOVA), and one-way (ANOVA) test was used to test variance chi-square for two-to-two comparisons between the groups. A non-parametric test was used when the distribution did not satisfy normality. Sample sizes were determined based on preliminary experiments and previous studies using similar methodologies, ensuring adequate power (≥ 80%) to detect anticipated effect sizes .Effect sizes with 95% confidence intervals for key data are shown in Table 1. SPSS 25.0 statistical software

**Table 1** Summary table of effect values with 95% confidence intervals for key data

| Figure/experiment | Comparison groups | Measurement | Effect value (mean difference/fold change) | 95% CI | *P*-value |
|---|---|---|---|---|---|
| Figure S3A | PC vs. Adjacent | PIEZO1 Expression | 5.15 | 3.78 to 7.52 | < 0.0001 |
| Figure S3B | PC vs. Adjacent | Co-localization of PIEZO1 and MUC1 | 19.75 | 12.56 to 24.94 | < 0.0001 |
| Figure 3A | Yoda1 vs. NC | Wound Healing Area (%) | 25.8% | 21.3% to 30.3% | < 0.001 |
| Figure 3A | GsMTx4 vs. NC | Wound Healing Area (%) | -18.2% | -22.7% to -13.7% | < 0.001 |
| Figure 3B | Yoda1 vs. NC | Number of Invasive Cells | 8.54 | 7.21 to 9.87 | < 0.001 |
| Figure 3B | GsMTx4 vs. NC | Number of Invasive Cells | -6.23 | -7.56 to -4.90 | < 0.001 |
| Figure 4A | Yoda1 vs. NC | NGF mRNA (Fold Change) | 2.8 | 2.3 to 3.3 | < 0.001 |
| Figure 4A | Yoda1 vs. NC | BDNF mRNA (Fold Change) | 3.2 | 2.7 to 3.7 | < 0.001 |
| Figure 4A | Yoda1 vs. NC | GDNF mRNA (Fold Change) | 2.5 | 2.1 to 2.9 | < 0.001 |
| Figure 5A | Yoda1 vs. NC | Neuronal Chemotactic Migration Cell Count | 4.76 | 39.2 to 56.0 | < 0.001 |
| Figure 5B | Yoda1 vs. NC | Neuronal Invasion Cell Count | 6.38 | 54.1 to 73.5 | < 0.001 |
| Figure 5C | Yoda1 vs. NC | Adhesion Fluorescence Intensity (%) | 35.2% | 28.7% to 41.7% | < 0.001 |
| Figure 6E | Yoda1 vs. NC | YAP1 Total Protein (Fold Change) | 2.1 | 1.8 to 2.4 | < 0.001 |
| Figure 6F | Yoda1 vs. NC | YAP1 Nucleocytoplasmic Ratio | 2.4 | 2.0 to 2.8 | < 0.001 |
| Figure 6G | Yoda1+Verte. vs. Yoda1 | Neuronal Invasion Cell Count | -5.83 | -6.92 to -4.74 | < 0.001 |
| Figure 7C | GsMTx4 vs. Control | Tumor Weight (g) | -0.38 | -0.52 to -0.24 | < 0.01 |

was used for analysis. $p < 0.05$ was considered a statistically significant difference.

## Results

### The expression of PIEZO1 is abnormally increased in pancreatic cancer tissue and correlates with perineural infiltration

To observe the role of PIEZO1 in pancreatic cancer, an analysis was conducted of the data from the TCGA and GTEx databases. This analysis revealed that, among the various cancer types, PIEZO1 was found to be highly expressed in diffuse large B-cell lymphoma, glioblastoma, head and neck squamous cell carcinoma, pancreatic carcinoma, tenosynovial giant cell tumours, thymoma. In the context of pancreatic adenocarcinoma, the PIEZO1 expression level was significantly higher than adjacent normal pancreatic tissues, exhibiting approximately threefold higher levels (Fig. S1A). Secondly, the data demonstrated a correlation between elevated PIEZO1 expression and reduced disease-free survival in pancreatic cancer patients (Fig. S1B). Furthermore, analysis of the annotated UMAP cell subpopulation map of the downscaled pancreatic cancer single-cell data clustering revealed that PIEZO1 expression was predominantly observed in cancer cells, fibroblasts, and various immune cell types (Fig. 1A). In summary, by bioinformatics analysis, we found that PIEZO1 expression was abnormally elevated in pancreatic cancer, which may be a marker of poor prognosis in pancreatic cancer. Furthermore, correlation analysis was performed on data from pancreatic cancer samples in the TCGA database, revealing a positive correlation between PIEZO1 expression and various neurotrophic factors, including NGF, BDNF, GDNF, and NT3/NT-4 (Fig. 1B).

Subsequently, we undertook a spatial transcriptomic analysis of clinical pancreatic cancer tissue samples (Fig. S2A-B). The results demonstrated that the expression level of PIEZO1 in the nerve-infiltrating area was significantly higher than that in the non-nerve-infiltrating area, and the expression level gradually decreased from the nerve-infiltrating proximal area to the nerve-infiltrating distal area (Fig. 2A). Immunohistochemical staining was performed on tumour tissues from pancreatic cancer patients and adjacent pancreatic tissues to validate these findings further. The results demonstrated that the expression level of PIEZO1 was significantly higher in pancreatic cancer tissues than in adjacent non-cancerous tissues (Fig. 2B and Fig. S3A). Of particular note was the finding that PIEZO1 was enriched explicitly in the invaded perineurium (Fig. 2C). To delineate further the cell types expressing PIEZO1, we employed a combination of fluorescence co-localization staining of pancreatic cancer cell markers MUC1 and PIEZO1, along with S100β staining to label nerves. This analysis revealed a significant overlap between the MUC1 and PIEZO1 staining patterns, particularly adjacent to invaded nerves (Fig. 2D and Fig. S3B). Thus, PIEZO1 represents a potential therapeutic target to inhibit PNI in pancreatic cancer.

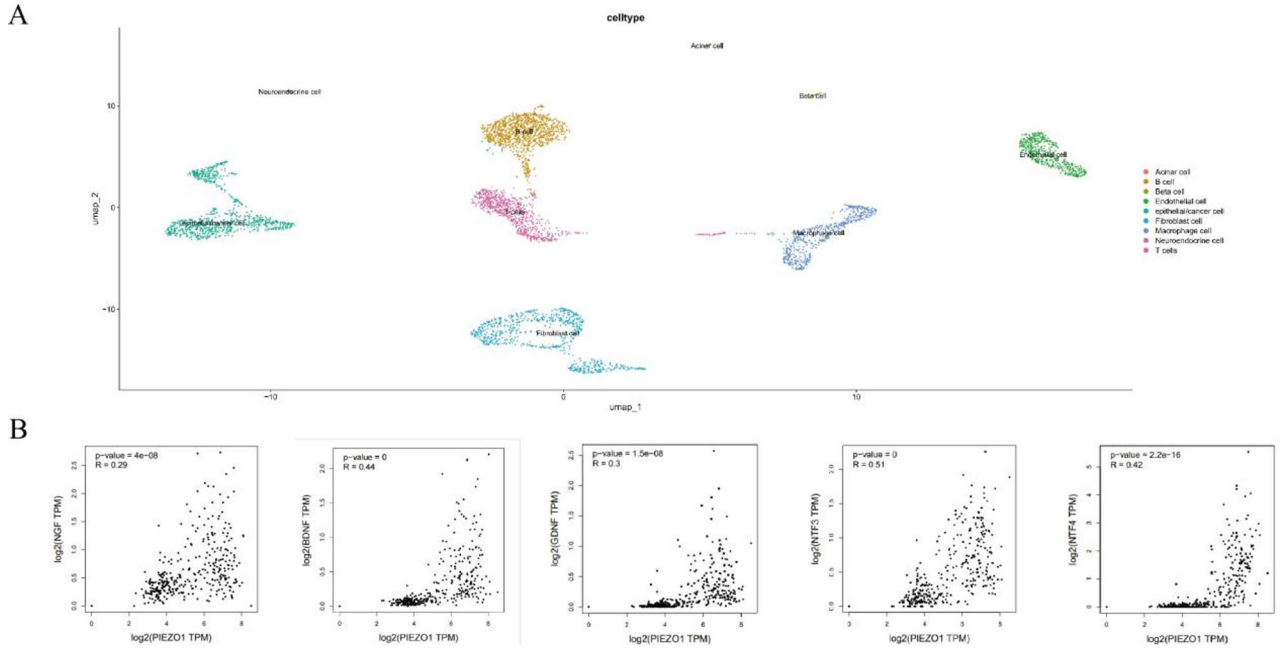



**Fig. 1** The expression level of PIEZO1 is related to neurotrophic factors. **A**: Subpopulation maps of UMAP cells annotated by downscaling clustering of pancreatic cancer single-cell data. **B**: Analysis of Pearson's correlation coefficients between PIEZO1 and various neurotrophic factors

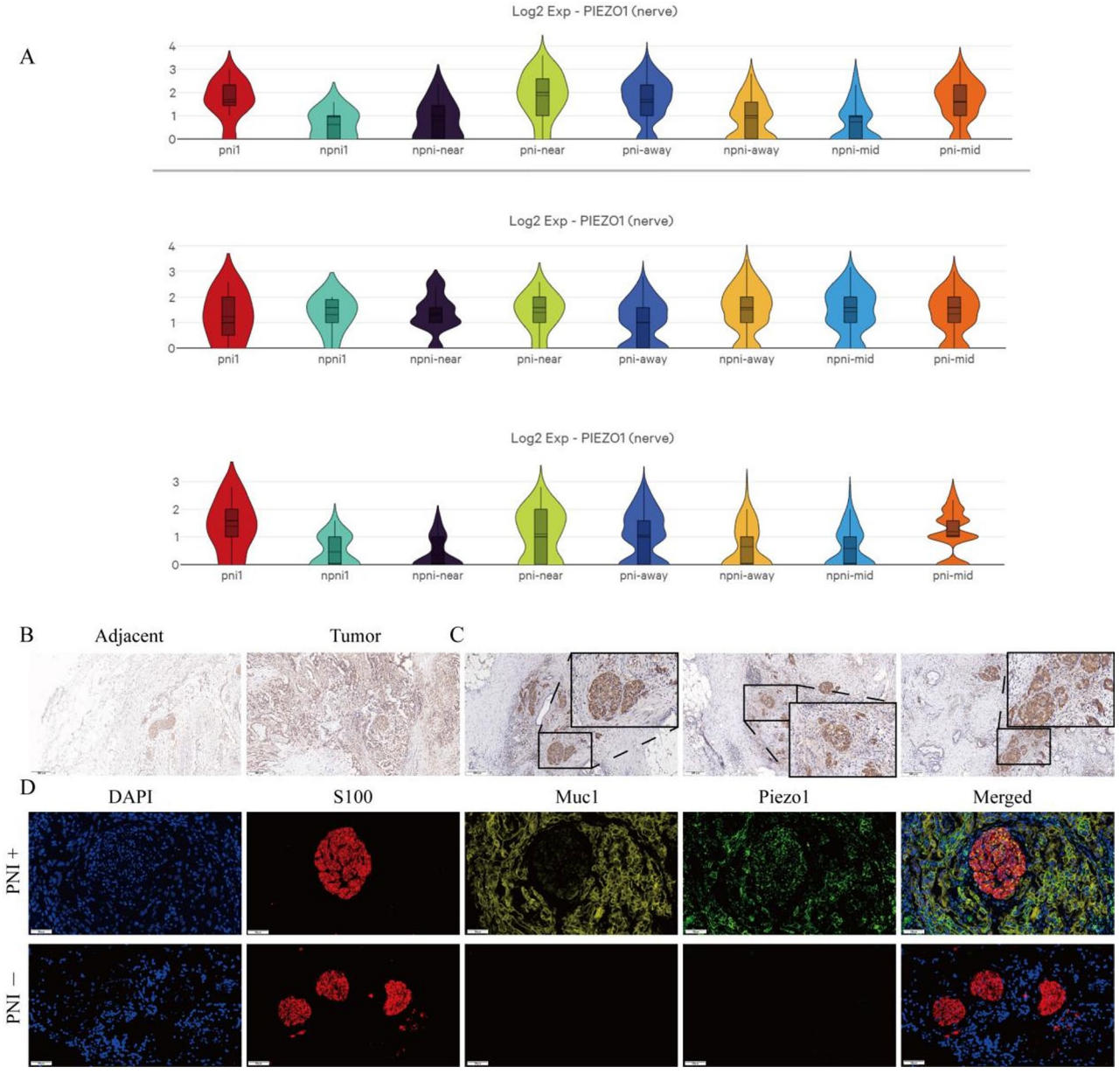



**Fig. 2** Clinical pancreatic cancer tissue samples to verify PIEZO1 expression level and localization. **A**: violin plot indicating PIEZO1 expression levels in different regions of pancreatic cancer; **B**: immunohistochemical analysis of PIEZO1 expression in pancreatic cancer tissues versus paraneoplastic tissues; **C**: immunohistochemical analysis of PIEZO1 expression next to the invaded nerves; **D**: use of immunofluorescence for perineural PIEZO1 localization (PIEZO1 (green) vs. MUC1 + cancer cells (yellow) in S100β + nerves (red))

### The activation of PIEZO1 has been demonstrated to play a pivotal role in enhancing the migration and invasiveness of pancreatic cancer cells

The effects of PIEZO1 on the migration and invasion ability of pancreatic cancer cells were investigated using the healing and transwell invasion assays. The preliminary experiment results indicated that the optimal intervention concentration was 10 μM for Yoda1 and 2.5 μM for GsMTx4 (Fig. S4). The scratch assay revealed that the wound area exhibited significant healing in the agonist Yoda1 group. In contrast, the healed area was diminished in the inhibitor group, GsMTx4, in comparison to the negative control (NC) group (Fig. 3A). The Transwell invasion assay demonstrated that more cells traversed the compartment in the presence of the agonist, while fewer cells traversed the compartment in the presence of the inhibitor (Fig. 3B). Western blot analysis showed that Yoda1 treatment downregulated E-cadherin and upregulated N-cadherin, consistent with EMT activation. (Fig. 3C). These findings, characterized by E-cadherin downregulation and N-cadherin upregulation, together with the observed enhancement of migration and invasion, are

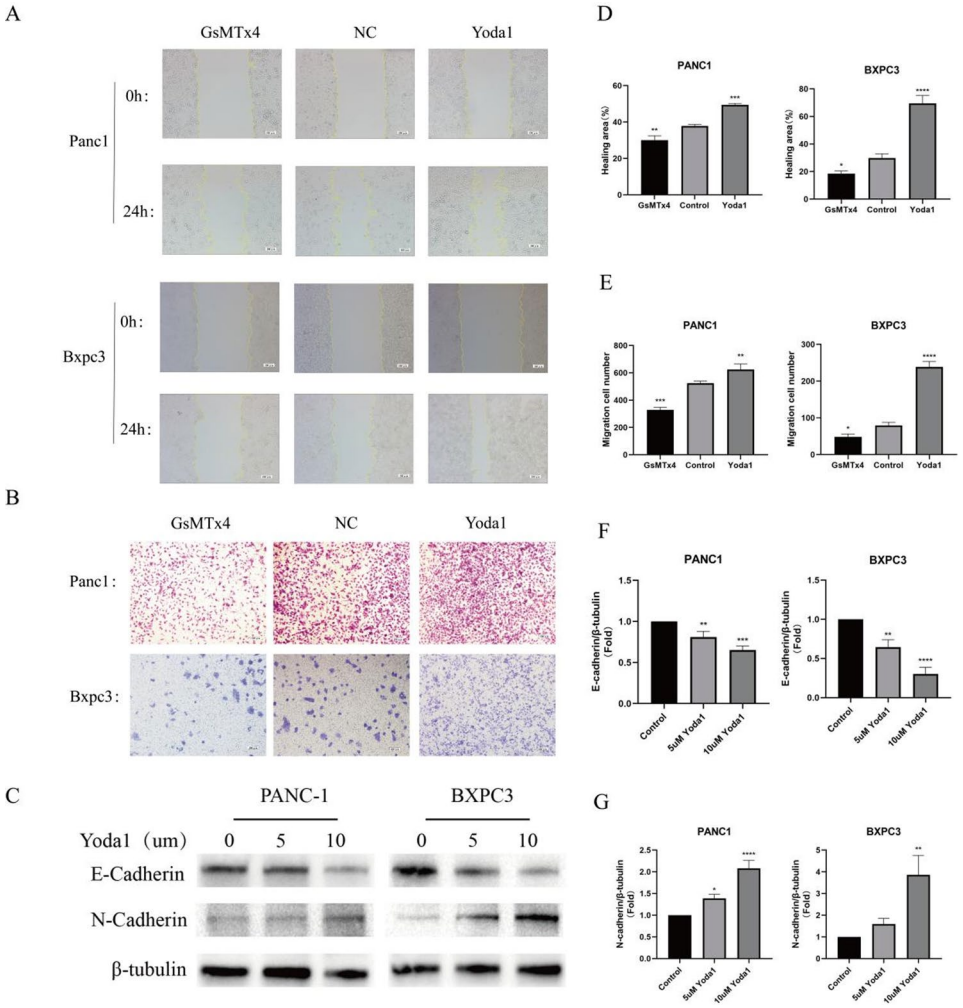



**Fig. 3** Effect of PIEZO1 on functional assays related to migration and invasion of pancreatic cancer cells. **A**: Scratch assay to assess the effect of PIEZO1 on the migratory ability of pancreatic cancer cells; **B**: Transwell assay to detect the effect of PIEZO1 on the invasive ability of pancreatic cancer cells; **C**: WESTERN BLOT results showed that the expression levels of EMT representative molecules were changed; **D-G**: Scratch area, the number of invasive cells, and the grey value of the lanes were examined using ImageJ software quantified. All the data are presented as the means ± SDs: *represents $p < 0.05$, ** represents $p < 0.01$, ***represents $p < 0.001$, ****represents $p < 0.0001$

consistent with the induction of an EMT-like phenotype in pancreatic cancer cells upon PIEZO1 activation. The statistical outcomes of each experiment (Fig. 3D-G). In summary, activation of PIEZO1 promotes the migration and invasion ability of pancreatic cancer cells.

### The activation of PIEZO1 is a key factor in promoting neurotrophic function in pancreatic cancer

Neurotrophic factors are frequently regarded as indicators to assess cancer cells' neuroinvasive capacity. For this study, the most common neurotrophic factors were selected for experimentation: NGF, BDNF, GDNF, and NRTN. Utilising the agonist Yoda1 to target pancreatic cancer cells, RT-qPCR analysis revealed augmented expression of NGF, BDNF, and GDNF. At the same time, no substantial alterations were detected for NRTN (Fig. 4A). To validate these findings; we employed WESTERN BLOT analysis, which corroborated the RT-qPCR results (Fig. 4B). Undifferentiated PC12 cells are a cell line that is highly sensitive to neurotrophic factors, expresses nerve growth factor receptors, and can produce a neural phenotype in response to neurotrophic factors. Under conventional culture conditions, undifferentiated PC12 cells were typically rounded with no discernible surface protrusions. However, a small number of protrusions (indicated by red arrows) were observed to form on the surface of PC12 cells using a cancer cell culture medium as the conditioned medium. Furthermore, when PC12 cells were cultured using a Yoda1-activated cancer cell culture medium, an increased number of protrusions formed on the surface of the cells, and these protrusions were also longer. In addition, there was a clear appearance of neuron-like cells (Fig. 4C), Which suggests that

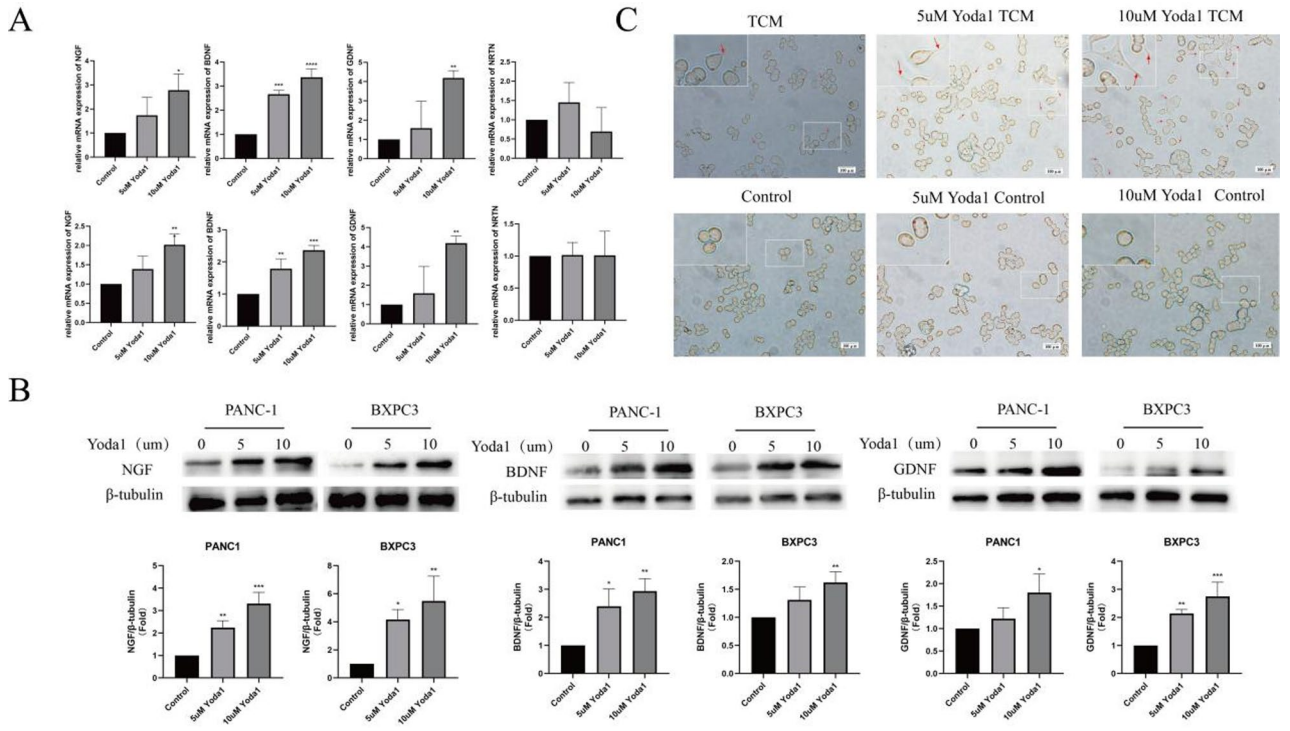



**Fig. 4** Effect of PIEZO1 on neurotrophic function in pancreatic cancer. **A**: RT-qPCR to detect the relationship between PIEZO1 activation and neurotrophic factors; **B**: WESTERN BLOT to detect the relationship between PIEZO1 activation and neurotrophic factors; **C**: Schematic representation of the effect of cancer cell supernatant on axon formation in undifferentiated PC12 cells (shown by red arrows). All the data are presented as the means ± SDs: * represents $p < 0.05$, ** represents $p < 0.01$, *** represents $p < 0.001$, **** represents $p < 0.0001$

PIEZO1 promotes neurotrophic function in pancreatic cancer cells.

### The activation of PIEZO1 promotes neurophilic function in pancreatic cancer cells

An in vitro model of PNI in pancreatic cancer was constructed by co-culturing the PDAC cell line and PC12 cells. A nerve migration model was built using the Transwell co-culture system. The results showed that more cells crossed the compartment in the presence of agonists and fewer cells crossed the compartment in the presence of inhibitors (Fig. 5A). A nerve invasion model was constructed using matrix gel-embedded PC12 cells, which demonstrated an increase in cells invading the matrix gel in the agonist group and the opposite in the inhibitor group (Fig. 5B). Furthermore, neural adhesion experiments demonstrated that the activation of PIEZO1 enhanced the adhesion ability of cancer cells to PC12 cells in comparison with the control group. At the same time, the inhibition of PIEZO1 reduced the adhesion ability of cancer cells to PC12 cells (Fig. 5C). The statistical outcomes of each experiment (Fig. 5D-F). In summary, the findings of this study demonstrate that activation of PIEZO1 promotes the neurophilic function of pancreatic cancer cells.

### YAP1 is a transcriptional target of PIEZO1 signalling in pancreatic cancer cells

The RNA-Seq sequencing results were used to functionally categorise the differential genes by GO enrichment and to focus on some of the genes related to cell migration, neuronal function, and the extracellular matrix (Fig. 6A). KEGG pathway enrichment analysis showed that PIEZO1 was involved in the cancer MAPK pathway, the Hippo pathway, the TGF-β pathway, and the glycine and serine amino acid metabolic regulation (Fig. 6B). YAP1 is a major effector of the Hippo pathway. As a mechanosensitive transcriptional regulator situated at the end of the path, it can control the expression of downstream genes. Given the observed correlation between PIEZO1 and the Hippo signalling pathway and the shared mechanosensing characteristics of PIEZO1 and Yap1, it was hypothesised that PIEZO1 expression might be associated with Yap signalling. In the spatial transcriptome mapping of pancreatic cancer nerve-infiltrating tissues, PIEZO1 and Yap1 expression regions were found to be highly overlapping, suggesting that there may be a close connection between the two (Fig. 6C). Following the activation of pancreatic cancer cells using Yoda1, a significant upregulation of Yap1 expression was observed within the cells (Fig. 6E). Furthermore, immunofluorescence analysis revealed that Yoda1 activation resulted in

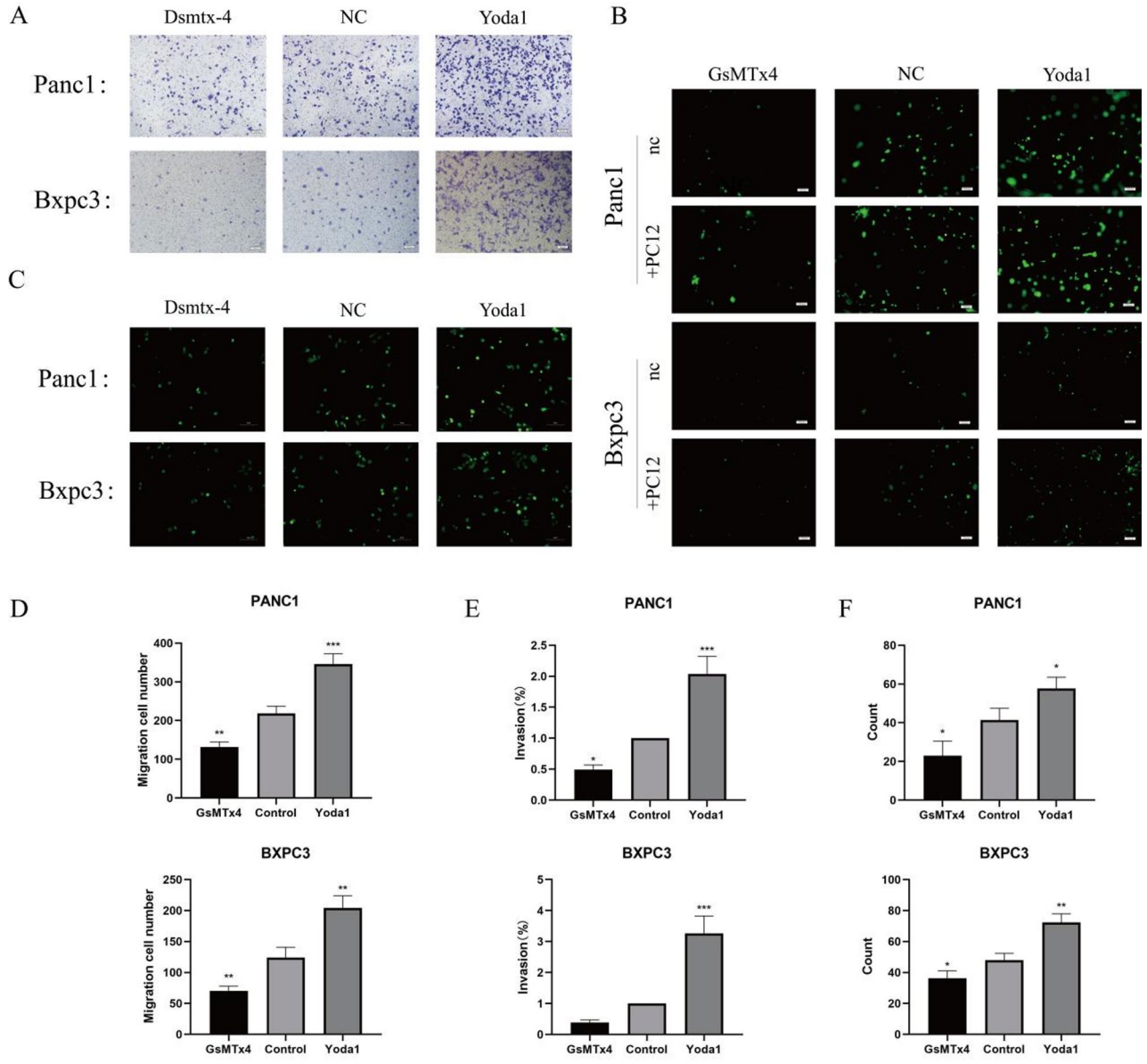



**Fig. 5** Effect of PIEZO1 on neurophilic function-related experiments in pancreatic cancer cells. **A**:Changes in the migratory ability of pancreatic cancer cells to nerve cells under the action of the agonit Yoda1 with the inhibitor GsMTx4; **B**: Changes in the invasive ability of pancreatic cancer cells to nerve cells under the action of the agonist Yoda1 with the inhibitor GsMTx4; **C**: Changes in the adhesion ability of pancreatic cancer cells to nerve cells under the action of the agonist Yoda1 with the inhibitor GsMTx4D-F: Quantification of the number of invaded cells, fluorescence intensity using ImageJ software. All the data are presented as the means ± SDs; *represents $p < 0.05$, ** represents $p < 0.01$, *** represents $p < 0.001$

increased nuclear localization of Yap1 in pancreatic cancer cells (Fig. 6D). To validate the findings above further, nucleoplasmic separation experiments were performed, and the protein levels of Yap1 in the nucleus and cytoplasm were detected by WB (Fig. 6F). The results indicate a robust activation of YAP1 signaling upon PIEZO1 stimulation.

To verify further the hypothesis that Yap is involved in regulating the neuroinvasive ability of pancreatic cancer by PIEZO1, a PIEZO1 agonist was used in conjunction with a Yap inhibitor, Verteporfin, in treating pancreatic cancer cells. It was demonstrated that in the experimental group receiving the combination of Yoda1 and Verteporfin, the neuroinvasive ability of the pancreatic cancer cells was effectively suppressed by Verteporfin (Fig. 6G). This finding suggests that the activation of PIEZO1 to promote neuroinvasion of pancreatic cancer cells is at least partially dependent on the activation of the Yap1 signalling pathway.

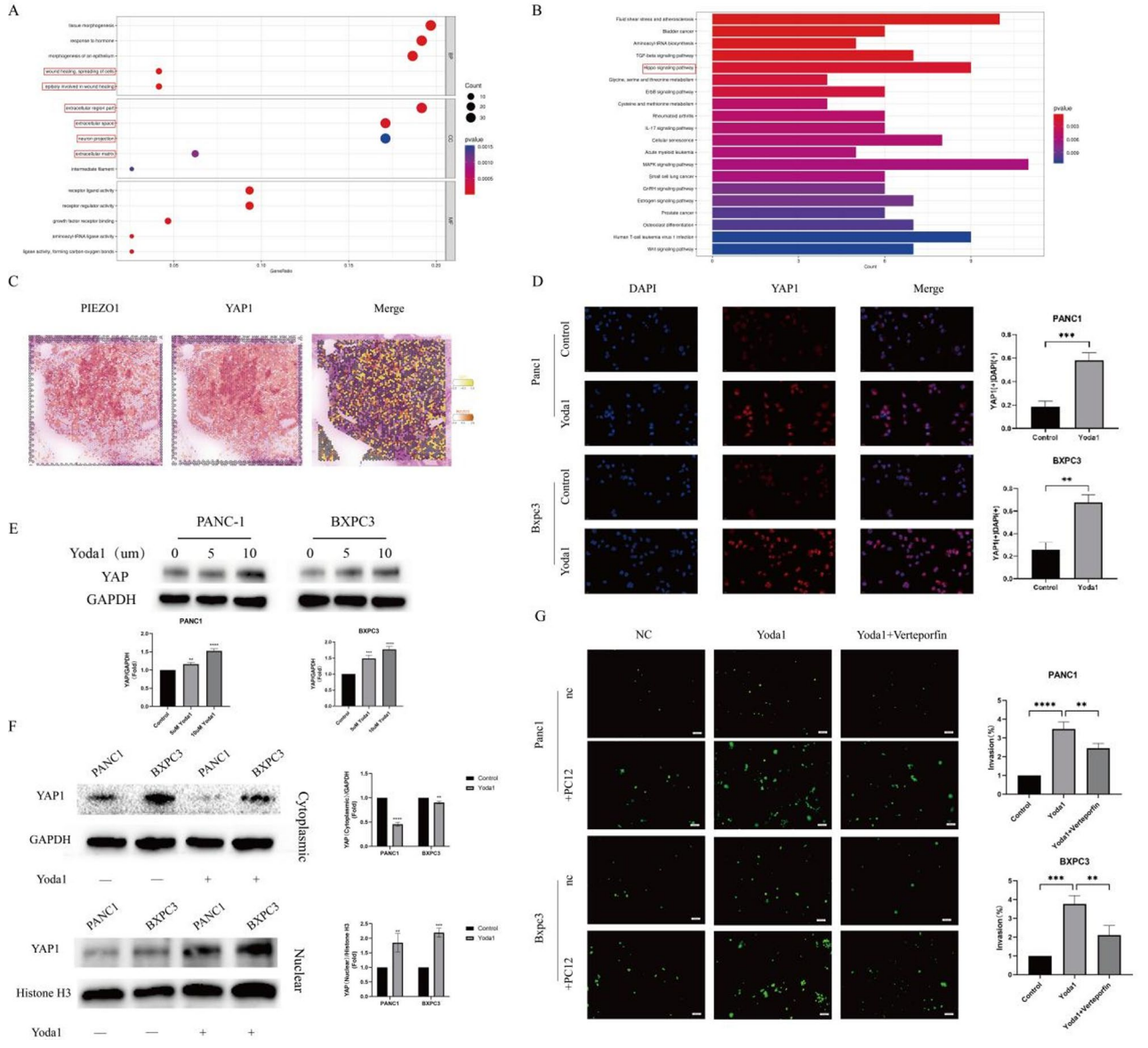
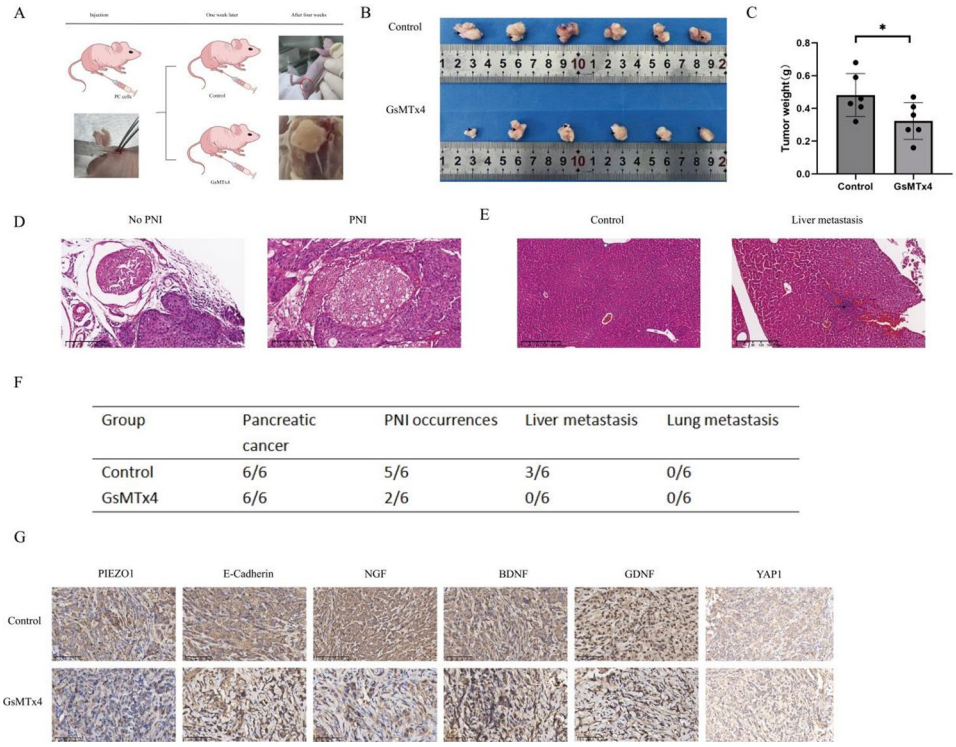



**Fig. 6** Transcriptome reveals that PIEZO1 may play a key role through YAP1. **A**: GO functional enrichment of transcriptomic differential genes; **B**: KEGG pathway enrichment of differential genes; **C**: Target gene mapping analysis of pancreatic cancer nerve infiltration tissue samples; **D**: YAP1 localisation analysis using immunofluorescence; **E**: WESTERN BLOT detection of total YAP1 expression level; **F**: WESTERN BLOT detection of YAP1 expression level in nucleus and cytoplasm respectively; **G**: Co-culture model to detect the invasive ability of pancreatic cancer on nerve cells. **G**: Co-culture model to detect the invasive ability of pancreatic cancer on neuronal cells. all the data are presented as the means ± SDs; *represents $p < 0.05$, ** represents $p < 0.01$, ***represents $p < 0.001$, ** **represents $p < 0.0001$

### Targeting PIEZO1 inhibits PNI in vivo

A xenograft model of pancreatic cancer origin was constructed and divided into control and inhibitor groups. Experimental procedures and tumour tissues were obtained (Fig. 7A). Upon completion of the study, nude mice were euthanised, and tumour samples were collected and weighed. GsMTx4 treatment significantly reduced tumour burden compared with controls (Fig. 7B–C). The sciatic nerve is indicated by black arrows. Histopathological examination of H&E-stained sections revealed a striking difference in the pattern of perineural invasion between the groups. In the control group, tumor cells were observed to tightly encircle and aggressively infiltrate the sciatic nerve bundle. In stark contrast, tissues from the GsMTx4-treated group consistently exhibited a clear histological cleavage plane between the tumor mass and the nerve, with no evidence of nerve bundle invasion (Fig. 7D). Histopathologic analysis also showed the presence of liver metastases in the control group (Fig. 7E), and none of the lung metastases occurred. The incidence of PNI with liver and lung metastases in each group (Fig. 7F). IHC staining




| Group | Pancreatic cancer | PNI occurrences | Liver metastasis | Lung metastasis |
|---|---|---|---|---|
| Control | 6/6 | 5/6 | 3/6 | 0/6 |
| GsMTx4 | 6/6 | 2/6 | 0/6 | 0/6 |

**Fig. 7** Targeting PIEZO1 to inhibit PNI in vivo. **A**: Establishment of sciatic nerve PNI xenograft model; **B**: Tumour samples. Black arrow: sciatic nerve embedded in the tumour mass; **C**: Weight of nerve invasion tumour samples; D: HE, nerve invasion tumour samples; **E**: HE, liver metastasis in the sciatic nerve infiltration model. Black arrows: tumour metastasis; **F**: Tumour formation, PNI occurrence, liver metastasis and lung metastasis status in the nerve infiltration model; **G**: immunohistochemical analysis of target gene expression levels. All the data are presented as the means ± SDs; * represents $p < 0.05$

was performed to verify the changes in the expression of PIEZO1 and YAP1, as well as the differences in the expression of various neurotrophic factors and EMT-related molecules, which further confirmed the reliability of the in vitro experiments (Fig. 7G).

## Discussions

PNI is a distinct metastatic route in PDAC, often occurring independently of vascular or lymphatic spread and serving as a key determinant of poor prognosis and severe neuropathic pain [23, 24]. While the biomechanical properties of the PDAC microenvironment—notably increased matrix stiffness—have been implicated in cancer aggressiveness, the molecular mechanisms linking mechanical cues to PNI remain incompletely defined. Here, we identify the mechanically sensitive ion channel PIEZO1 as a potential regulator of pancreatic cancer neurotropism, and it may promote the neuroinfiltration behavior of cancer cells through the transcriptional regulator YAP1.

Our spatial transcriptomic and immunohistochemical analyses revealed that PIEZO1 expression is significantly enriched in pancreatic cancer tissues, particularly in regions adjacent to invaded nerves, and correlates with poor patient survival. Co-localization studies further confirmed PIEZO1 expression predominantly in cancer cells, supporting its cell-autonomous role in PNI. These findings are consistent with prior reports of PIEZO1 upregulation in PDAC and its function as a mechanosensor responsive to stromal stiffness [21, 25].

Functionally, activation of PIEZO1 induced a molecular and functional shift in pancreatic cancer cells, characterized by cadherin switching and heightened migratory/invasive capacity, hallmarks of an EMT-like process, alongside the upregulation of neurotrophic factors NGF, BDNF, and GDNF. These effects were abrogated by pharmacological inhibition of PIEZO1, underscoring its role in modulating a neurotropic phenotype. Importantly, we found that PIEZO1-induced neurotropism may be mediated through the Hippo pathway effector YAP1. Transcriptomic profiling and immunofluorescence assays demonstrated that PIEZO1 activation promotes YAP1 nuclear translocation. Moreover, the YAP1 inhibitor verteporfin effectively suppressed PIEZO1-driven neural invasion, confirming the functional relevance of this axis. Our results align with emerging evidence that YAP1, as a mechanotransductive transcription factor, can be activated by PIEZO1-mediated $Ca^{2+}$ influx in other cancers [26–28]. To our knowledge, this is the first study to map and functionally validate a PIEZO1–YAP1 axis inside the perineural niche that converts mechanical cues into pro-invasion signals. Furthermore, our KEGG analysis

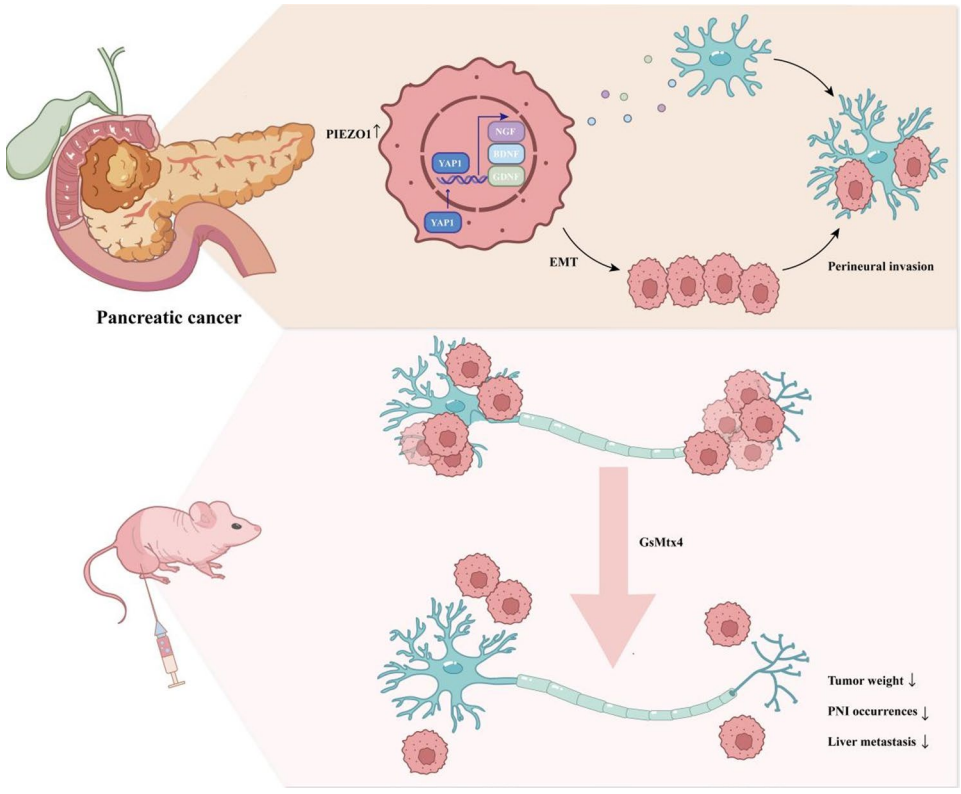



**Fig. 8** PIEZO1-Enhanced Neurotropism

indicated PIEZO1's association with MAPK and TGF-β pathways alongside Hippo signaling. This aligns with the emerging concept of mechano-signaling networks, where these pathways frequently interact. Notably, cross-talk between Hippo–YAP and MAPK/ERK or TGF-β–Smad signaling has been documented to cooperatively regulate cell invasion and matrix remodeling in cancer [29, 30]. Thus, while our data highlight the pivotal role of the Hippo–YAP axis, PIEZO1 may potentially coordinate a broader signaling network to promote the neurotropic phenotype. Future studies dissecting the hierarchy and synergy among these pathways will provide a more comprehensive understanding of mechanotransduction in PNI.

Despite these insights, several limitations of our study warrant consideration. First, while we employed well-established pharmacological tools (Yoda1 and GsMTx4) to modulate PIEZO1, genetic validation using knockout or knockdown models would strengthen the causal relationship between PIEZO1 and YAP1 activation [31–33]. Second, the use of PC12 cells, though widely accepted for neurotropic assays, may not fully recapitulate the complexity of human neural interactions [34, 35]. Future studies employing human dorsal root ganglion neurons or patient-derived co-cultures would enhance physiological relevance. Third, although spatial transcriptomics revealed a PIEZO1 expression gradient that peaked in perineural regions, the analysis was restricted to three patient samples, a limitation inherent to the technology. The gradient was nevertheless reproduced in an independent immunohistochemical cohort. Larger spatially resolved datasets will be required to delineate compartment-specific PIEZO1 signaling during pancreatic-cancer neuroinvasion. Finally, the sciatic nerve injection model, though highly relevant for PNI studies, does not fully mimic spontaneous pancreatic tumorigenesis. Orthotopic or genetically engineered PDAC models may provide broader context for PIEZO1 function in tumor progression and metastasis [36, 37].

Translational application of PIEZO1 inhibition also faces challenges [38]. GsMTx4, while a well-established tool compound for mechanosensitive channel blockade, is not fully specific to PIEZO1 and can also inhibit other mechanosensitive channels (e.g., Piezo2 and certain TRP channels). Its poor stability and limited tissue penetration further preclude clinical application. These off-target and pharmacokinetic limitations mean that the observed in vivo effects of GsMTx4—though consistent with our in vitro PIEZO1 loss-of-function phenotypes—should be interpreted with caution. Developing selective PIEZO1 antagonists or targeting downstream effectors like YAP1 represents a potential therapeutic strategy that requires future investigation. Several YAP/TAZ inhibitors are currently under preclinical investigation and may hold

promise for disrupting the PIEZO1–YAP1 axis in PDAC [39–41]. Beyond the PNI focus, future work should explore whether PIEZO1–YAP1 signaling influences the immune microenvironment, given YAP's established role in fostering immunosuppressive niches [42]. Integrating mechanobiology with immunomodulation may uncover novel combination strategies for this recalcitrant malignancy.

## Conclusions

In conclusion, the present findings suggest that the PIEZO1-YAP1 axis could represent a potential contributor to pancreatic cancer progression and neuroinvasion. In contrast to other tumour pro-metastatic mechanisms, PIEZO1 in pancreatic cancer is specifically dependent on Yap1-mediated secretion of EMT and neurotrophic factors (Fig. 8). This difference may be related to the unique rigid microenvironment of pancreatic cancer. Further in-depth study of the molecular mechanism of this axis and its interaction with other signalling pathways is recommended to facilitate a more comprehensive understanding of the malignant biological behaviour of pancreatic cancer and provide a rationale for future research into therapeutic strategies targeting mechanosignaling pathways in pancreatic cancer. Future studies should further explore the specific mechanism of action of the PIEZO1-YAP1 axis in pancreatic cancer and the prospect of its translational application.

## Supplementary Information

The online version contains supplementary material available at https://doi.org/10.1186/s12935-026-04244-z.

Supplementary Material 1.

**Acknowledgements**
Not applicable.

**Author contributions**
All authors contributed to the study conception and design. Material preparation, data collection and analysis were performed by Jinhong Li, Yuqing Zheng, Ling Wang, Juan Tang, Shangeng Weng, and Renfeng Xu. The first draft of the manuscript was written by Jinhong Li, Feng Gao and Qicai Liu. All authors commented on previous versions of the manuscript. All authors read and approved the final manuscript.

**Funding**
This work was supported by the National Natural Science Foundation of China (No. 82172953 to Feng Gao), National Natural Science Foundation of Fujian (No. 2024Y9158) and National Key Clinical Specialty Construction Project Fund (No. 2022YBL-ZD-02 to Feng Gao). These funding sources played key supportive role for sample collection, molecular analysis of patient samples, bioinformatics analysis.

**Data availability**
The data that support the findings of this study are available on request from the corresponding author.

## Declarations

**Ethics approval and consent to participate**
All the techniques used in this study met the requirements of Medical Ethics Committee of the First Affiliated Hospital of Fujian Medical University 2018 [053] and 2024 [714].

**Consent for publication**
Not applicable.

**Competing interests**
The authors declare no competing interests.

Received: 26 August 2025 / Accepted: 20 February 2026
Published online: 09 March 2026

**References**

1. Bray F, Laversanne M. Sung H, Global cancer statistics 2022: GLOBOCAN estimates of incidence and mortality worldwide for 36 cancers in 185 countries [J]. CA Cancer J Clin. 2024;74(3):229–63.
2. Hosein AN, Brekken RA, Maitra A. Pancreatic cancer stroma: an update on therapeutic targeting strategies [J]. Nat reviews Gastroenterol Hepatol. 2020;17(8):487–505.
3. Truong LH, Pauklin S. Pancreatic cancer microenvironment and cellular composition: current understandings and therapeutic approaches [J]. Cancers. 2021;13(19):5028.
4. D'haese JG, Hartel M, Demir IE, et al. Pain sensation in pancreatic diseases is not uniform: the different facets of pancreatic pain [J]. World J Gastroenterol. 2014;20(27):9154–61.
5. Zhu M, Luo F, Xu B, et al. Research Progress of Neural Invasion in Pancreatic Cancer [J]. Curr Cancer Drug Targets. 2024;24(4):397–410.
6. Li J, Kang R. Cellular and molecular mechanisms of perineural invasion of pancreatic ductal adenocarcinoma [J]. Cancer Commun (London England). 2021;41(8):642–60.
7. Demir IE, Friess H, Ceyhan GO. Neural plasticity in pancreatitis and pancreatic cancer [J]. Nat reviews Gastroenterol Hepatol. 2015;12(11):649–59.
8. Zhang H, Li S, Liu S, et al. Therapeutic targeting of cell death-immune crosstalk in cancer to rewire the tumor immune microenvironment [J]. Mol Cancer. 2025;24(1):277.
9. Zhang P, Zhang M, Liu J et al. Mitochondrial Pathway Signature (MitoPS) predicts immunotherapy response and reveals NDUFB10 as a key immune regulator in lung adenocarcinoma [J]. J Immunother Cancer. 2025;13(7):e012069.
10. Itoh Y, Takehara Y, Kawase T, et al. Feasibility of magnetic resonance elastography for the pancreas at 3T [J]. J Magn Reson imaging: JMRI. 2016;43(2):384–90.
11. Hupfer A, Brichkina A, Koeniger A, et al. Matrix stiffness drives stromal autophagy and promotes formation of a protumorigenic niche [J]. Proc Natl Acad Sci USA. 2021;118(40):e2105367118.
12. Deng B, Zhao Z. Biological role of matrix stiffness in tumor growth and treatment [J]. J translational Med. 2022;20(1):540.
13. Han B, Guan X. Stiffened tumor microenvironment enhances perineural invasion in breast cancer via integrin signaling [J]. Cell Oncol (Dordrecht). 2024;47(3):867–82.
14. Shen T, Li Y, Wang D, et al. YAP1-TEAD1 mediates the perineural invasion of prostate cancer cells induced by cancer-associated fibroblasts [J]. Biochim et Biophys acta Mol basis disease. 2022;1868(12):166540.
15. Liu T, Yu S, Zhang L, et al. Yes-associated protein 1 in cancer: bridging mechanical transduction and epigenetic regulation [J]. Volume 26. Cancer biology & therapy. 2025:2562726. 1.
16. Pathak MM, Nourse JL, Tran T, et al. Stretch-activated ion channel Piezo1 directs lineage choice in human neural stem cells [J]. Proc Natl Acad Sci USA. 2014;111(45):16148–53.
17. Gudipaty SA, Lindblom J, Loftus PD, et al. Mechanical stretch triggers rapid epithelial cell division through Piezo1 [J]. Nature. 2017;543(7643):118–21.
18. Qin L, He T, Chen S, et al. Roles of mechanosensitive channel Piezo1/2 proteins in skeleton and other tissues [J]. Bone Res. 2021;9(1):44.
19. Coste B, Mathur J, Schmidt M, et al. Piezo1 and Piezo2 are essential components of distinct mechanically activated cation channels [J]. Volume 330. Science (New York, NY); 2010. pp. 55–60. 6000.

20. Moccia F, Fiorio Pla A, Lim D et al. Intracellular Ca(2+) signalling: unexpected new roles for the usual suspect [J]. Frontiers in physiology. 2023;14(1210085).
21. Zhu Z, Li W, Gong M et al. Piezo1 act as a potential oncogene in pancreatic cancer progression [J]. Life sciences. 2022;310(121035).
22. Acheta J, Bhatia U. Piezo channels contribute to the regulation of myelination in Schwann cells [J]. Glia. 2022;70(12):2276–89.
23. Marchesi F, Piemonti L, Mantovani A, et al. Molecular mechanisms of perineural invasion, a forgotten pathway of dissemination and metastasis [J]. Cytokine Growth Factor Rev. 2010;21(1):77–82.
24. Ferdoushi A, Griffin N. Tumor innervation and clinical outcome in pancreatic cancer [J]. Sci Rep. 2021;11(1):7390.
25. Song Y, Chen J, Zhang C, et al. Mechanosensitive channel Piezo1 induces cell apoptosis in pancreatic cancer by ultrasound with microbubbles [J]. iScience. 2022;25(2):103733.
26. Baroja I, Kyriakidis NC, Halder G, et al. Expected and unexpected effects after systemic inhibition of Hippo transcriptional output in cancer [J]. Nat Commun. 2024;15(1):2700.
27. Liu S, Xu X, Fang Z et al. Piezo1 impairs hepatocellular tumor growth via deregulation of the MAPK-mediated YAP signaling pathway [J]. Cell calcium, 2021;95(102367).
28. Mao J, Yang R, Yuan P et al. Different stimuli induce endothelial dysfunction and promote atherosclerosis through the Piezo1/YAP signaling axis [J]. Archives of biochemistry and biophysics, 2023;747(109755).
29. Paul S, Hagenbeek TJ, Tremblay J, et al. Cooperation between the Hippo and MAPK pathway activation drives acquired resistance to TEAD inhibition [J]. Nat Commun. 2025;16(1):1743.
30. Chapeau EA, Sansregret L, Galli GG, et al. Direct and selective pharmacological disruption of the YAP-TEAD interface by IAG933 inhibits Hippo-dependent and RAS-MAPK-altered cancers [J]. Nat cancer. 2024;5(7):1102–20.
31. Botello-Smith WM, Jiang W, Luo Y, et al. A mechanism for the activation of the mechanosensitive Piezo1 channel by the small molecule Yoda1 [J]. Nat Commun. 2019;10(1):4503.
32. Mo J, Zhang Y, Cao C, et al. Activation of mechanosensitive ion channel Piezo1 linking metabolic reprogramming and pro-inflammatory responses in hepatocellular carcinoma [J]. Cell communication signaling: CCS. 2025;23(1):280.
33. Zhang X, Jiang E, Fu W, et al. Engineered endoplasmic reticulum-targeting nanodrugs with Piezo1 inhibition and promotion of cell uptake for subarachnoid hemorrhage inflammation repair [J]. J Nanobiotechnol. 2025;23(1):274.
34. Cheng K, Pan J, Liu Q, et al. Exosomal lncRNA XIST promotes perineural invasion of pancreatic cancer cells via miR-211-5p/GDNF [J]. Oncogene. 2024;43(18):1341–52.
35. Lu WL, Kuang H, Gu J et al. GAP-43 targeted indocyanine green-loaded near-infrared fluorescent probe for real-time mapping of perineural invasion lesions in pancreatic cancer in vivo [J]. Nanomedicine: nanotechnology, biology, and medicine. 2023;50(102671).
36. Tian Z, Su M, Yu M, et al. KRAS/ACTN4/p65-NR2A axis mediates glutamine-glutamate metabolic coupling between schwann cells and pancreatic cancer promoting perineural invasion [J]. Journal of advanced research; 2025.
37. Li T, He R, Tian Q, et al. Cancer-associated fibroblast-derived circKLHL24 drives perineural invasion in pancreatic cancer via dual regulation of the sec31a-CXCL12 axis [J]. J experimental Clin cancer research: CR. 2025;44(1):281.
38. Thien ND, Hai-Nam N, Anh DT et al. Piezo1 and its inhibitors: Overview and perspectives [J]. European journal of medicinal chemistry. 2024;273(116502).
39. Zhou R, Wang H, Bai C, et al. Targeted degradation of endogenous YAP by nanobody bioPROTAC inhibits tumor progression [J]. Nat Commun. 2025;16(1):9374.
40. Zhou J, Yu C, Yang W, et al. Recent Advances in Combination Therapy of YAP Inhibitors with Physical Anti-Cancer Strategies [J]. Biomolecules. 2025;15(7):945.
41. Liu J, Bai W, Zhou T, et al. SDCBP promotes pancreatic cancer progression by preventing YAP1 from β-TrCP-mediated proteasomal degradation [J]. Gut. 2023;72(9):1722–37.
42. Su N, Lian W, Zhang B, et al. Inhibiting NEDD4 in triple-negative breast cancer cells reprograms tumor immune microenvironment via the β-TrCP/YAP/ECM axis [J]. Cell Rep Med. 2025;6(10):102420.


## Publisher's note

Springer Nature remains neutral with regard to jurisdictional claims in published maps and institutional affiliations.